

SIMULATION OF UNSTEADY SHIP AIRWAKES USING OPENFOAM

Weixing Yuan, Richard Lee, and Alanna Wall

National Research Council (NRC) Canada, Ottawa, Ontario, K1A 0R6, Canada

Weixing.Yuan@nrc-cnrc.gc.ca

Keywords: *Unsteady aerodynamics, ship airwakes, computational fluid dynamics (CFD)*

Abstract

To aid pilot training for shipboard helicopter operations, computational fluid dynamics (CFD) is increasingly being performed to model ship airwakes. The calculated velocity field data are exported to the flight simulator as look-up tables. In the Canadian context, work to expand ship airwake simulation capabilities is currently being done using the freeware OpenFOAM. The current paper reports on the progress of this work using a simple frigate shape (SFS2), which is a highly simplified ship geometry, to validate the method for static cases. By employing Delayed Detached Eddy Simulations (DDES), OpenFOAM was able to compute the unsteady ship airwakes reasonably compared to the available wind tunnel data. After the validation, OpenFOAM was applied to a more representative example: the Canadian Patrol Frigate (CPF). Hybrid structured and unstructured grids were used because of the complexity of the CPF geometry. The agreement between the computed and the experimental results for the CPF was not as reasonable as the agreement of the SFS2 results, indicating that further development of the CPF simulation is required.

1 Introduction

The operation of helicopters from and onto naval ships is a challenging task for pilots. The launch and recovery of helicopters is often performed from the landing decks of small ships, which are subject to random motion in six degrees of freedom. The difficulty is increased owing to the fact that the landing deck is immersed in the unsteady ship airwake. Because

of the nature of bluff-body aerodynamics, the separated flow and sheared vortices interact, resulting in a time-varying airwake with highly turbulent structures, which can significantly intensify the difficulty associated with a launch and recovery manoeuvre.

As flight simulation technologies mature, simulators are being used increasingly to aid pilot training for shipboard helicopter operations. A key area that affects simulation fidelity is the modelling of ship airwakes. The determination of airwake characteristics is not a trivial task. At-sea and wind tunnel measurements can be used to provide data from which airwake models can be generated. Increasingly, computational fluid dynamics (CFD) is used for modelling ship airwakes. In this approach, CFD solves the flow over the ship, and the resulting velocity field data are exported to a flight simulator as look-up tables. In Canada, work to expand ship airwake simulation capabilities is currently being done using the freeware OpenFOAM. OpenFOAM was selected for its cost effectiveness and its flexibility, which may allow future studies involving ship motion. The current paper reports on the progress of this work, using an updated version of a simple frigate shape (SFS2) to validate the method for static cases. The application of the methodology to the Canadian Patrol Frigate (CPF), which is a representative geometry, is also demonstrated.

2 Computational Setup for the SFS2

To develop confidence with OpenFOAM, computations were performed for the SFS2, a simplified ship geometry which was proposed

originally by a ship airwake modelling working group within The Technical Co-operation Program (TTCP), to facilitate the development of CFD capabilities for ship airwakes. Figure 1 shows the ship configuration; details of the geometry are described by Zan [1].

As part of the development of the SFS2, its airwake was characterized experimentally in the NRC 2 m \times 3 m wind tunnel using hot-film anemometers for a 1:100 scale model of the geometry, as shown in Figure 1. This SFS2 configuration has also been investigated numerically by a number of researchers with commercial CFD codes. Syms [2] and Zhang et al. [3] performed Reynolds-averaged Navier-Stokes (RANS) simulations for the SFS2 model. Forrest and Owen [4] performed detached eddy simulations (DES) at full scale. The Reynolds number dependence or scaling effect has not been evaluated since it is generally assumed that the flow over such bluff body structures is insensitive to Reynolds number.

The purpose of this work is to validate the results produced by OpenFOAM [5] against experimental data and to determine whether OpenFOAM is suitable for ship airwake simulations. OpenFOAM was applied to compute the three-dimensional (3D) unsteady incompressible flows over the SFS2. The OpenFOAM pressure-based Navier-Stokes solver, Pimple, was used in this study. OpenFOAM applies the integral form of the conservation laws of mass and momentum on an unstructured grid. A fully-implicit, second-order temporal differencing scheme was implemented in the discretization. The discretization of the convective and diffusive fluxes was carried out in a co-located variable arrangement using a finite-volume approach, which was second-order accurate in space. The coupling of the pressure and velocity was handled using a modified SIMPLE algorithm in the Pimple computations. Because of the nature of the bluff-body aerodynamics, the Spalart-Allmaras delayed detached eddy simulation (DDES) was employed to model the turbulence.

A C-H type structured grid was used in this study. The farfield of the computational domain was set at $5l_s$ and the depth of the domain was set to $0.75l_s$, where l_s represents the total length

of the ship. These parameters are comparable to $4.5l_s$ and $0.75l_s$, respectively, which were used by Forrest and Owen for their cylindrical mesh [4]. Although OpenFOAM is designed for unstructured grids, we have used a structured grid because the geometry of SFS2 is not complex. The structured grid helped reduce the amount of mesh cells and improved the quality of the grid. The outer farfield boundary was set as an inlet or outlet, depending on the local flow direction. Both upper and lower surfaces were set as slip boundary conditions. The ship surface was modeled as a wall with a no-slip boundary condition. Forrest and Owen have conducted grid convergence studies for the same geometry [4]. Corresponding to their medium grid, the grid developed in the current work has six million cells; as a result, the maximum spacing normal to the wall gave averaged wall unit values of $y^+ \sim 65$ (near the front edge of the superstructure). This number is significantly higher than the conventional requirement ($y^+ \sim 1$) for attached flows. As will be seen later, this did not adversely affect the accuracy of the results because the ship airwake flow is mainly inertia-driven and the separation points are fixed by the sharp edges rather than caused by boundary layer separation.

As Zan [6] pointed out, reasonable agreement between CFD and experiment at one wind angle cannot be considered as a complete validation for a CFD approach. In this study, computations were performed for a headwind and a Green 45° wind-over-deck (WOD) condition, and compared directly with the results from the corresponding wind tunnel study. In naval terminology, winds from starboard are denoted as “Green” and winds from port as “Red”. To be consistent with the wind tunnel experiments, the freestream velocity U_∞ was set to 60 m/s for the headwind case, and 50 m/s for the Green 45° WOD condition. In the wind tunnel study, data were collected at a frequency of 2,000 Hz, which corresponds to a timestep (Δt) of 5×10^{-4} seconds. Based on the non-dimensional timestep employed by Forrest and Owen [4] for their full scale simulations, a timestep of 4×10^{-5} seconds was used in the current work. The computations were started using this nominal timestep for the

headwind case. The resulting non-dimensional timesteps were $CFL_{\text{mean}} = 0.1$ and $CFL_{\text{max}} = 40$ for the headwind case and $CFL_{\text{mean}} = 0.07$ and $CFL_{\text{max}} = 200$ for Green 45° , respectively; with CFL_{max} at the pointed bow whereas $CFL \sim 1$ in the airwake. Further tests showed that the timestep could reach 1×10^{-4} seconds without encountering numerical instabilities while delivering reasonable results. Considering the consistency, all results reported in this paper were obtained using the nominal timestep, unless stated elsewhere. The computations were performed for eight seconds of physical time, resulting in 346 units of flow through time (l_s/U_∞), with 330 used for sampling.

In this study, ten pressure and velocity coupling Pimple iterations were performed per timestep as a standard. Increasing the number of iterations to 50 did not improve the accuracy of the solution. To accelerate the computations, the computational domain was decomposed into 64 blocks for parallel computations.

3 Computed SFS2 Results and Discussion

3.1 Mean Velocity

The velocities are expressed in the body axis. The origin of the body-axis coordinate system lies on the centreline of the flight deck at the intersection of the flight deck surface and the aft face of the hangar, as shown in Figure 1. The survey grid is termed Map 1 for the headwind case and Map 3 for the Green 45° condition. Figure 2 depicts mean velocity along a lateral plane located on Map 1c for a headwind case and Map 3c for the Green 45° WOD condition. The plane is located at 50% of flight deck length; laterally, the plane spans two beam widths, symmetrically about the centerline of the ship; and vertically, its height corresponds to 75% of hangar height and its elevation above the flight deck is 50% of hangar height. The location represents a spot at which a helicopter would be hovering during a landing maneuver. The computed results are comparable to the work of Forrest and Owen [4]. For comparison, their results are also plotted in Figure 2 (labelled as “Liverpool”).

For the headwind case, a reduction in longitudinal velocity can be seen near the centre, within the wake behind the hangar. Significant gradients exist in the time-averaged values of the velocity components which is believed to affect the trim of the helicopter. Despite the symmetric velocity distributions from CFD, compared with the slight asymmetric velocity distribution in the experiments, all of the trends measured in the wind tunnel data are generally replicated by the CFD. The maximum discrepancy of the mean velocity between the current CFD and the experimental results is approximately 3%, which represents excellent agreement.

The computations for the Green 45° case were more challenging. At Green 45° , the flow over the flight deck is dominated by separated flows from the windward vertical edge of the hangar and the windward deck edge, and a vortical structure formed at the corner of the windward edge of the hangar roof. Compared with the headwind case, the separated off-body flow region is larger and more complex. A comparison between CFD and wind tunnel results for the Green 45° WOD condition shows that the velocity distribution trends were qualitatively captured by the CFD. There are obvious differences in the longitudinal and lateral components of velocity; however, these differences are comparable to the results reported by Forrest and Owen [4] and Syms [2]. Forrest and Owen have suggested that the discrepancy may be attributed to a difference in the incident flow between the CFD and the experiment — this must be investigated further with parametric CFD studies. Nevertheless, the results from the present study agree well with those of Forrest and Owen; the agreement with the wind tunnel results is slightly better. In the latter case, the agreement is attributed to the fully structured grid used in the current study, as opposed to the unstructured grid employed in the work of Forrest and Owen.

Figure 3 illustrates the time-averaged longitudinal and lateral velocity distributions from the hot-film survey and the computations, on the four airwake planes over the flight deck for both the headwind and Green 45° cases. While the hot-film probe has good resolution

and fast response, it cannot differentiate between forward and reversing flows. Thus, experimental data in reverse flows are unreliable and are not shown in the figure. The data were non-dimensionalized by the freestream speed. The flow pattern at the headwind condition shows excellent agreement between the CFD and experimental results. A classic bluff-body wake arises in which a significant momentum deficit is observed above the flight deck. For the Green 45° condition, the CFD results show the correct trend in the flow pattern, in particular for the lateral velocity, with some differences for the longitudinal velocity, when compared with the experimental data.

3.2 Turbulence Intensity

Figure 4 shows the computed turbulence intensities compared with the wind tunnel data. In general, the present CFD slightly under-predicted the x-component while over-predicted the lateral one. As with the mean velocities, the computations are in better agreement with the experimental data for the headwind case when compared with the Green 45° case. This is attributed to the latter case having more complex flow physics. Although they were not an exact match in magnitude, the CFD and wind tunnel data featured consistent trends. As shown in the figure, the levels of turbulence increase monotonically as the flight deck is approached laterally. The increased turbulence will contribute to pilot workload as a helicopter approaches the flight deck from the lateral direction.

3.3 Spectral Characteristics

Figure 5 shows plots of power spectral density, where the velocity data have been recorded at point 31 on Map 1c for the headwind case and Map 3b for Green 45°. For both CFD and the experiments, the spectral characteristics were developed from time-series data, employing a Fourier transform algorithm within a 1,024-sampling window. The experimental velocity spectra represent an average of three runs; the sampling duration of each run was 16.4 seconds. The CFD simulations, however, were performed for a physical duration of eight seconds; as a

result, the CFD results exhibit more scatter. Nonetheless, the agreement between CFD and wind tunnel data is promising, both in terms of frequency content and power.

3.4 Pressure Distributions

Computational fluid dynamics has the advantage of acquiring data from a number of sample points simultaneously, allowing the computation of mean values and spatial correlations for both velocities and pressure. Although pressure data are not used as input for flight simulators, from a research perspective, the pressure field helps with the understanding of the flow physics. Figure 6 to Figure 8 illustrate the pressure distributions on the frigate surface and surrounding areas. The figures clearly show low and high pressure regions, reflecting separated flow, impingement and reattachment areas. Compared with the headwind case, the pressure field at the Green 45° WOD condition is more complex. The flow showed full three-dimensionality at both angles.

Pressure data was not acquired experimentally.

3.4 Freestream Turbulence Effects

Using the DDES model, the eddy viscosity ν_t and its model parameter $\tilde{\nu}$ need to be set at the freestream. During the course of the validation process, inconsistent setups between the two values were found to cause incorrect solutions of the flow field. In the present study, $\tilde{\nu}$ and ν_t were both set to 100ν , where ν is the laminar viscosity. Conventionally, turbulence is characterized by intensities and length scales. Similar to Ref. [7], the wind tunnel values in the freestream were calculated as follows:

$$\nu_t = \sqrt{3/2} C_\mu Tu L U_\infty, \quad (1)$$

where Tu represents turbulence intensity, L is the turbulence length scale, and U_∞ is the freestream speed. The constant C_μ is 0.09. Since the turbulence intensity of the wind tunnel is known, but the turbulence length scale is not, the turbulence length scale L was varied for

defining the turbulence viscosities in the freestream. There were marginal differences in the results for the headwind case. Figure 9 shows two sets of results from computations using $\Delta t = 1 \times 10^{-4}$ seconds at the Green 45° condition with assumptions of $L = 0.043b$ and $4.3b$, where b is the ship beam. The resulting turbulence viscosities were $\nu_t = 3\nu$ and 300ν , respectively. Although the different parameters did not change the mean velocity distribution (as in Figure 2), the spectral characteristics were affected, both in terms of frequency content and power. Accurate freestream turbulence characteristics of the wind tunnel will help define the effective turbulence viscosity and thus improve the numerical results.

4 Preliminary CPF Results

To demonstrate its applicability and constraints, OpenFOAM was applied to the Canadian Patrol Frigate. Figure 10 shows the CPF geometry [8]. Zan et al. carried out analysis of CPF airwakes, including a steady-state simulation for a modified CPF model [9] which exhibits several simplifications of the main superstructure features. The model used in the current study is more representative of the actual ship geometry and is shown in Figure 11. As in Ref. [9], the masts of the CPF were omitted in the present study because difficulties were encountered with meshing the complex geometry of the masts and computing the complicated flow field of multiple bluff bodies. Furthermore, the present simulations were performed in a time-accurate manner, which allows for the analysis of unsteadiness and turbulences in the airwake.

The computational setups were similar to those used in the SFS2 simulations. Owing to the complexity of some CPF features, unstructured grids were used near the ship, except in the airwake where a structured grid was employed. This form of hybrid grid should be readily extendable to the complete frigate, with the main mast included. The simulations were performed for a full-scale CPF to keep the solution values at a reasonable magnitude that was greater than machine zero. Owing to the complexity of the geometry, the grid consisted of 28 million cells. A uniform incoming flow

condition was assumed, similar to a ship moving forward in low winds. The freestream turbulence intensity was set to 10%, which is comparable to 9% measured in wind tunnel tests for a similar CPF model. In this study, computations were carried out for the headwind only. In a corresponding experiment conducted in a NRC wind tunnel, three spots, located at starboard, port side and mid deck, in the CPF airwake, were setup for velocity measurements (Figure 12). In addition to the fact that the main mast was included on the model for these experiments, some other small geometrical features differ between the two models such as radomes. Examples of these differences can be seen by comparing Figure 11 and Figure 12. Experience comparing wind tunnel data for these different configurations supports the idea that these models are similar enough in their airwake characteristics for the development of the CFD capabilities. Also, a turbulence generator was employed in the freestream to model representative conditions in the atmospheric boundary layer.

In Table 1 to Table 3 and Figure 13, the computed results are compared with the experimental data available for the CPF model. The experimental data have been scaled using the reduced frequency to match the full-scale conditions. In general, the CFD predicted the trends of the velocity distributions qualitatively. Quantitative discrepancies are observed. In particular, the present CFD simulations under-predicted the mean velocity at starboard, the velocity fluctuations, and the velocity spectral power densities. The computed power spectra decayed somewhat faster when compared with the experiments. The discrepancies are attributed to the linear-upwind schemes used to overcome the numerical instabilities encountered in the computations. These dissipative schemes smeared out some flow fluctuations. The omission of the main mast may also account for the discrepancies. In future work, the numerical accuracy is expected to be improved when higher order or less-dissipative numerical schemes are employed. Also, a high-fidelity main mast will be incorporated in the simulation.

Table 1 Mean velocities ($\bar{u}/U_\infty, \bar{v}/U_\infty, \bar{w}/U_\infty$) in the CPF flight deck wake

Probes	Experimental	CFD
1 (Starboard)	0.48, -0.07, -0.14	0.41, -0.02, -0.10
2 (Port)	0.69, 0.08, -0.18	0.73, 0.01, -0.14
3 (Mid)	0.73, 0.02, -0.13	0.78, 0.02, -0.15

Table 2 Velocity fluctuations ($u'/U_\infty, v'/U_\infty, w'/U_\infty$) in the CPF flight deck wake

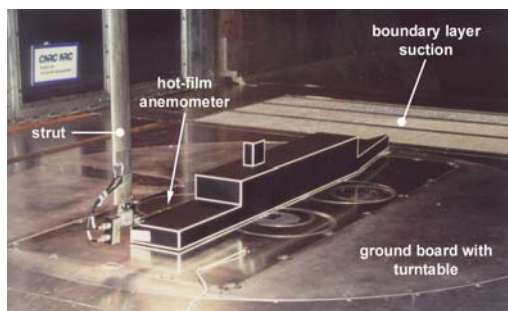
Probes	Experimental	CFD
1 (Starboard)	0.12, 0.16, 0.16	0.15, 0.14, 0.11
2 (Port)	0.14, 0.12, 0.10	0.14, 0.11, 0.08
3 (Mid)	0.14, 0.13, 0.10	0.08, 0.09, 0.08

Table 3 Turbulence intensity ($\sqrt{(u'^2 + v'^2 + w'^2)}/3/U_\infty$) in the CPF flight deck wake

Probes	Experimental	CFD
1 (Starboard)	0.14	0.14
2 (Port)	0.14	0.11
3 (Mid)	0.14	0.09

5 Concluding Remarks

The freeware OpenFOAM was validated for computations of three-dimensional unsteady incompressible ship airwake flows. Applying the Spalart-Allmaras DDES to model the turbulence, the computed results showed reasonable agreement with the wind tunnel data, demonstrating that the ability of OpenFOAM and the DDES model to capture important features in unsteady ship airwake flows. Additional convergence studies are needed to improve the computational accuracy so that the CFD results can be used to support applications for representative ship geometries. In particular, work to refine the linear-upwind scheme is in progress.



6 Acknowledgments

The present work was partially funded by the Defence Research and Development Canada (DRDC) and the Air Defense System (ADS) program of NRC. Dr. Chris Sideroff from the Applied CCM Canada provided technical support for the grid generation of the CPF.

References

- [1] Zan, S. On Aerodynamic Modelling and Simulation of the Dynamic Interface. *Proc Inst Mech Eng, Part G: J Aerospace Eng*, Vol. 219, No. 5, pp 393–410, 2005.
- [2] Syms, G. Simulation of Simplified-frigate Airwakes using a Lattice-Boltzmann Method. *J Wind Eng Ind Aerodynamics*, Vol. 96, No. 6-7, pp 1197–1206, 2008.
- [3] Zhang, F, Xu, H, and Ball, N. Numerical Simulation of Unsteady Flow over SFS 2 Ship Model. *47th AIAA Aerospace Sciences Meeting Including the New Horizons Forum and Aerospace Exposition*, Orlando, Florida, AIAA 2009-81, 5-8 January, 2009.
- [4] Forrest, J, and Owen, I. An Investigation of Ship Airwakes using Detached-Eddy Simulation. *Computers & Fluids*, Vol. 39, pp 656–673, 2010.
- [5] OpenFOAM. The Open Source CFD Toolbox. *User Guide*, Version 2.3.0, Feb. 2014.
- [6] Zan, S. Technical Comment on “Computational-Fluid-Dynamics Based Advanced Ship-Airwake Database for Helicopter Flight Simulation”. *AIAA Journal of Aircraft*, Vol. 40, No. 5, pp 1007, 2003.
- [7] Yuan, W, Poirel, D, Wang, B, and Benaissa, A. Effect of Freestream Turbulence on Airfoil Limit-Cycle Oscillations at Transitional Reynolds Numbers. *AIAA Journal of Aircraft*, Vol. 52, No. 4, pp 1214-1225, 2015.
- [8] https://en.wikipedia.org/wiki/Halifax-class_frigate.
- [9] Zan, S, Syms, G, Cheney, B. Analysis of Patrol Frigate Air Wakes. NATO RTO-AVT Symposium on Fluid Dynamics Problems of Vehicles Operating near or in the Air-Sea Interface, Amsterdam, The Netherland, 5-8 October 1998.

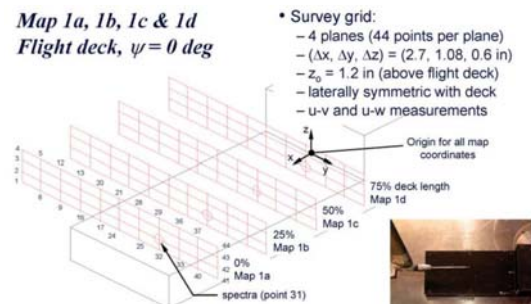
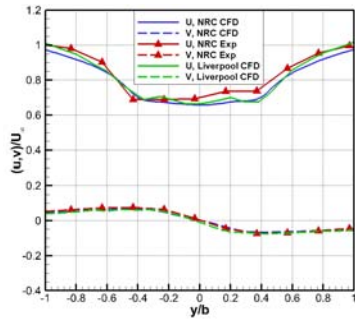
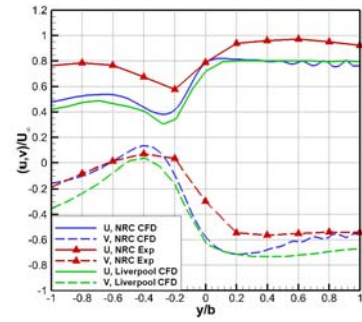


Figure 1. SFS2 model mounted inside the NRC 2 m x 3 m wind tunnel and the hot-wire survey grid over the flight deck.

SIMULATION OF UNSTEADY SHIP AIRWAKES USING OPENFOAM

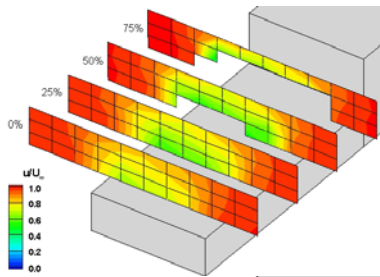


Headwind, Map 1c

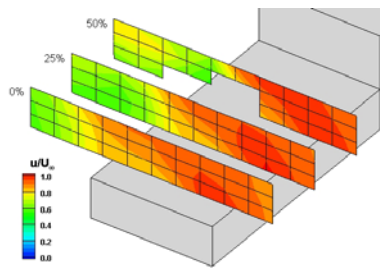
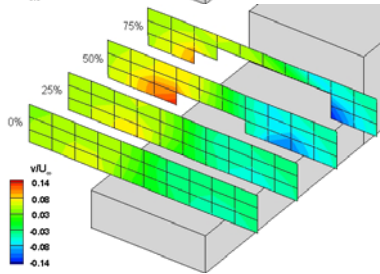


Green 45° wind, Map 3c

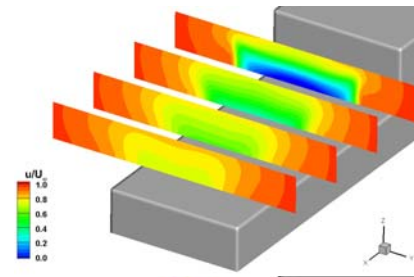
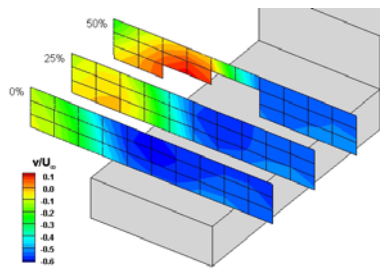
Figure 2. Mean velocity magnitudes normalized by freestream velocity U_∞ at 50% deck length (Maps 1c and 3c), plotted at hangar height. The lateral position is normalized by the ship beam b .



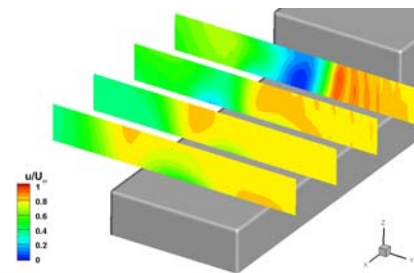
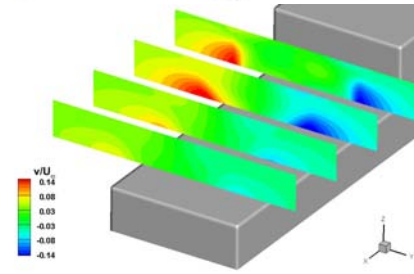
Headwind, Exp.



Green 45° wind, Exp.



Headwind, CFD



Green 45° wind, CFD

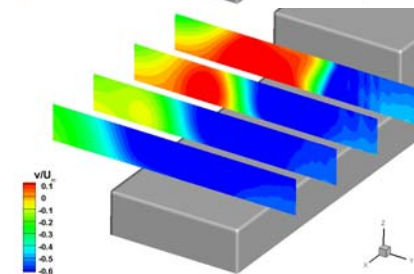


Figure 3. Mean velocity contours on off-body planes over the flight deck (Maps 1 and 3). The velocity is normalized by the freestream velocity.

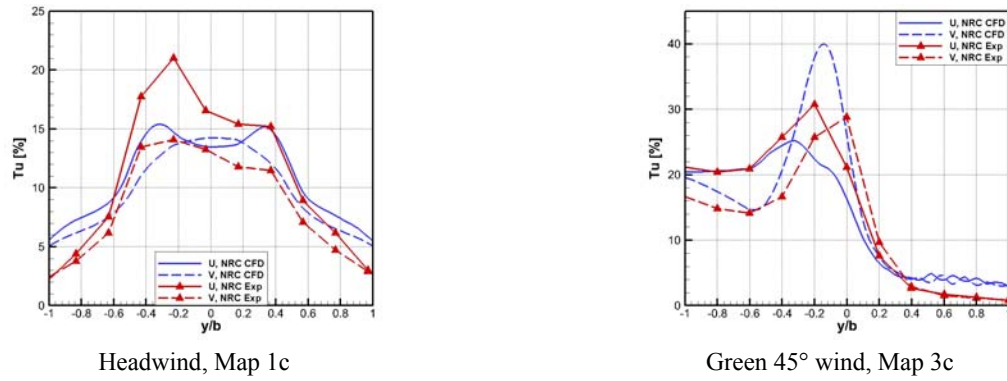


Figure 4. Turbulence intensities normalized by U_∞ at 50% deck length (Maps 1c and 3c), plotted at hangar height. The lateral position is normalized by the ship beam b .

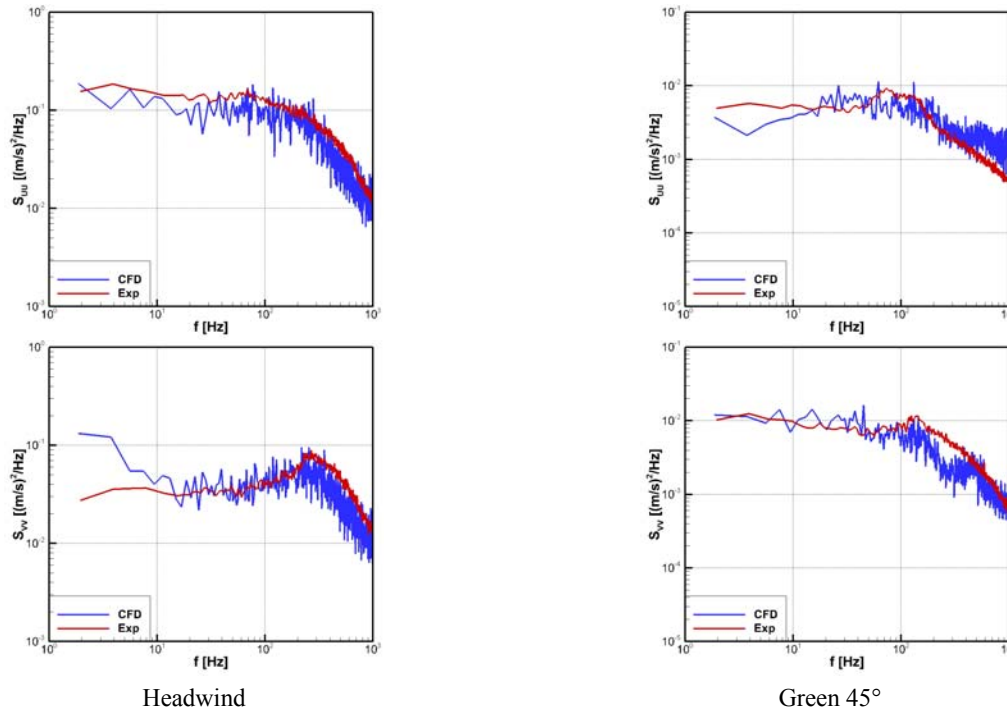


Figure 5. Power spectral density plots of longitudinal and lateral velocity components recorded at point 31 on Map 1c for headwind and Map 3b for Green 45° wind.

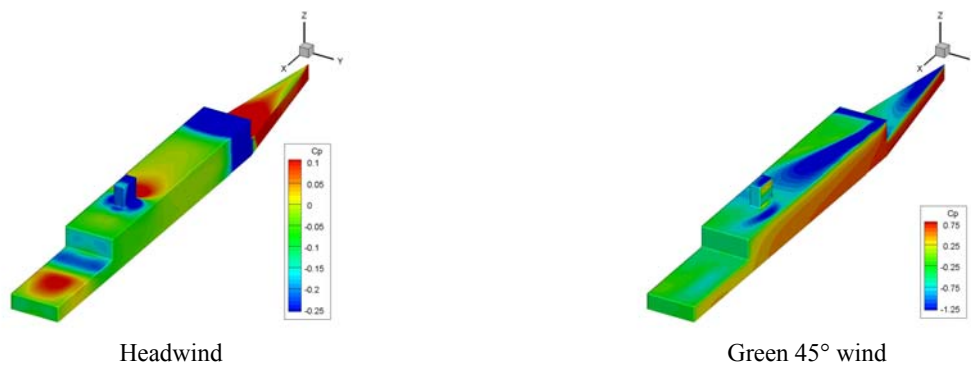


Figure 6. Mean pressure coefficient distribution on SFS 2 surfaces.

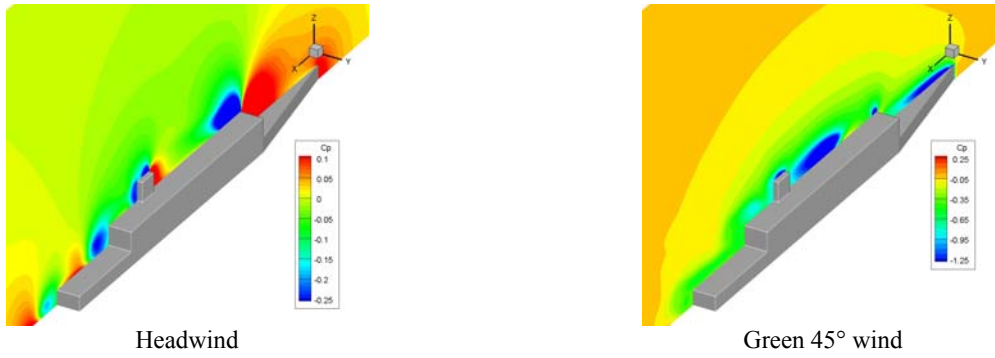


Figure 7. Mean pressure coefficient distribution on the mid plane at $Y = 0$.

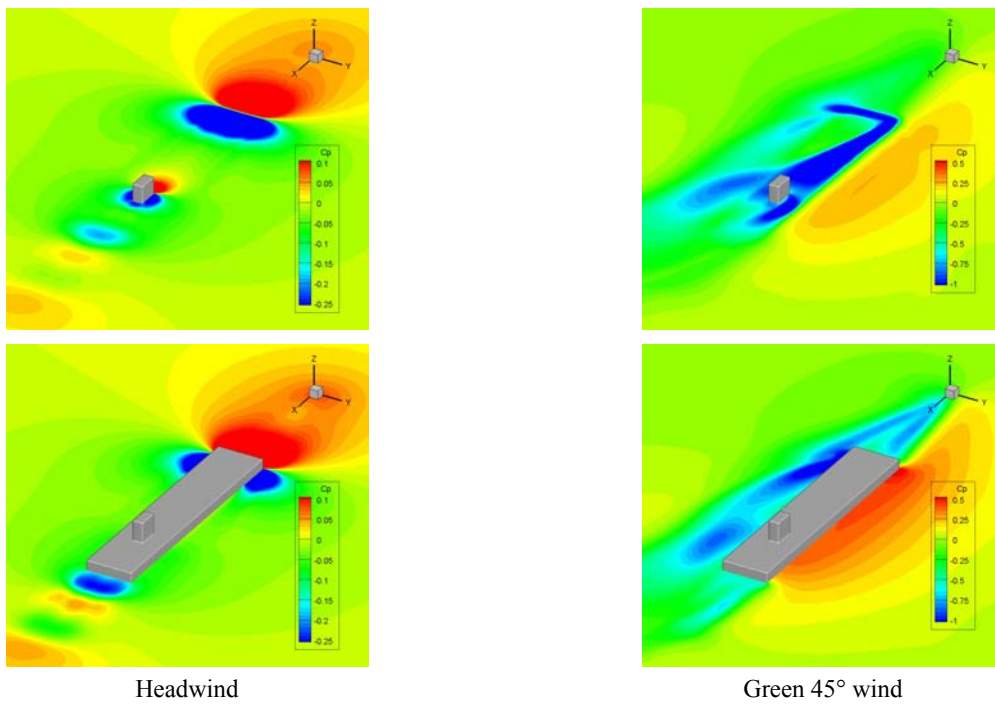


Figure 8. Mean pressure coefficient distribution on planes at $Z/h = 0.5$ (lower) and 1.5 (upper). The vertical position is normalized by the ship hangar height h .

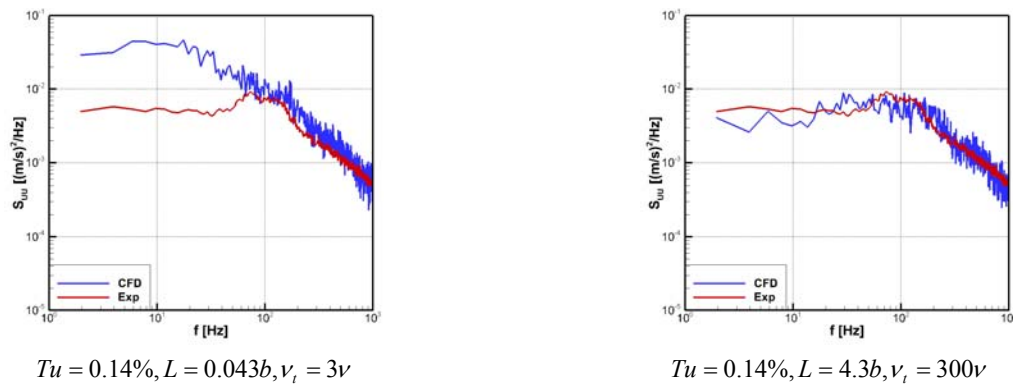


Figure 9. Freestream turbulence length scale effects for Green 45° wind, at point 31 on Map 3b. Turbulence viscosity at freestream is defined by $v_t = \sqrt{3/2} C_\mu TuLU_\infty$.



Figure 10. A Canadian patrol frigate launches a helicopter [8].

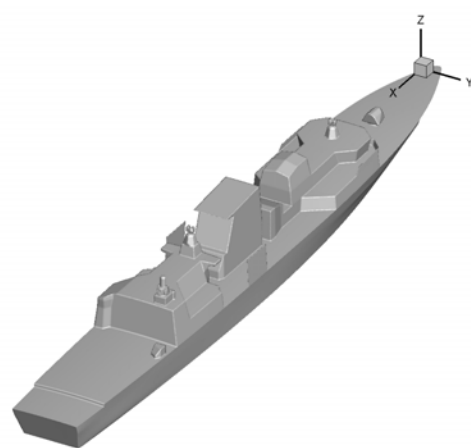
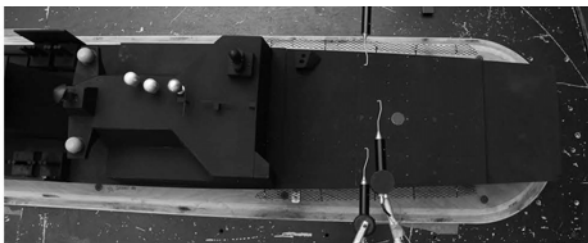
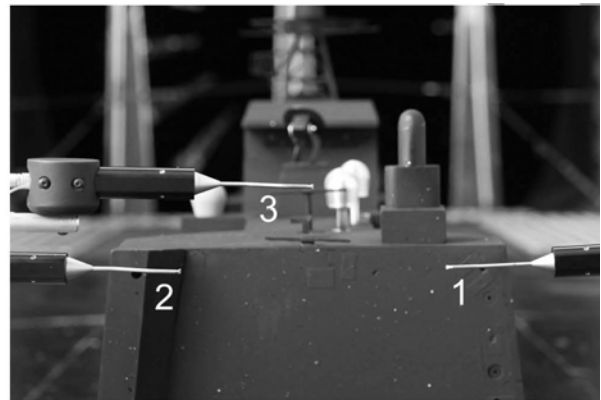


Figure 11. CPF model used in the CFD study.



Top view



Back view

Figure 12. Probe locations for airwake measurements for a CPF model in a NRC wind tunnel.

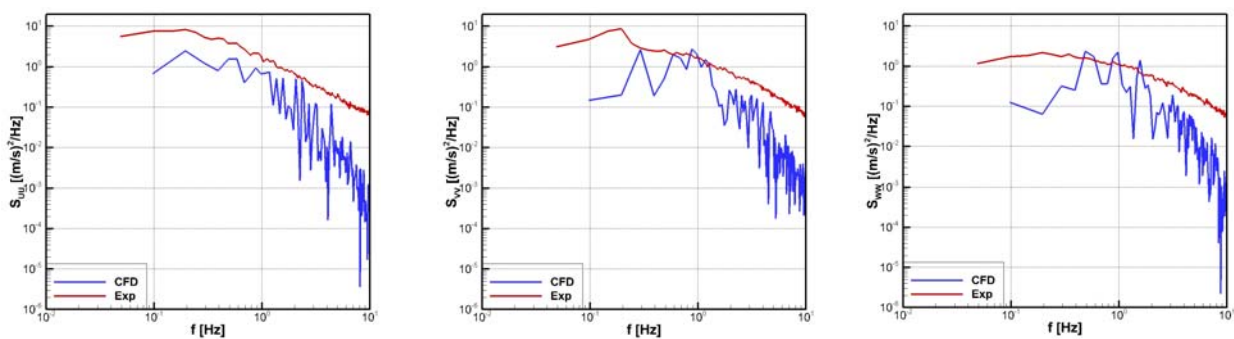


Figure 13. Power spectral density plots at probe 3 (mid-point) for the CPF.

Copyright Statement

The authors confirm that they, and/or their company or organization, hold copyright on all of the original material included in this paper. The authors also confirm that they have obtained permission, from the copyright holder of any third party material included in this paper, to publish it as part of their paper. The authors confirm that they give permission, or have obtained permission from the copyright holder of this paper, for the publication and distribution of this paper as part of the ICAS proceedings or as individual off-prints from the proceedings.